European Geothermal Congress 2022
Berlin, Germany | 17-21 October 2022
www.europeangeothermalcongress.eu

Approximate g-functions for selection of borehole field configurations used with ground-source heat pump systems

Timothy N. West[1], Jeffrey D. Spitler[1]

[1] School of Mechanical and Aerospace Engineering, Oklahoma State University, Stillwater, OK 74078 USA

spitler@okstate.edu

Keywords: ground heat exchangers, ground-source heat pump systems.

ABSTRACT

The arrangement of boreholes in ground heat exchangers used with ground-source heat pump systems is commonly based on pre-computed libraries of g-functions with standard configurations, e.g. placing the boreholes on a uniformly-spaced rectangular grid. Particularly for larger fields with many boreholes in situations with significant annual heat rejection/extraction imbalance, these configurations may be far from optimal. That is, depending on the space constraints, it may be possible to reduce the number of boreholes and amount of drilling required by shifting the positions of the boreholes to make better use of the available space. These configurations of boreholes are unlikely to be found in any library. Furthermore, manual arrangement of boreholes in complex-shaped fields is tedious and time-consuming for the engineer. Therefore, tools are needed that can automatically arrange boreholes in candidate configurations to fit the available land area, calculate the g-function for these configurations, select the best configuration, and determine the required depth for the best configuration. These tools need to be reasonably fast in order to be practical for the design engineer.

This paper reports on a fast method for calculating approximate g-functions using non-uniform segments and pre-computed integral tables. Despite being "approximate" g-functions, the difference between a g-function calculated with a more detailed method and the approximate g-function is usually under 1% RMSE. The g-functions for borehole fields with 300, 500, and 1000 boreholes can be calculated in about 2, 6, and 30 seconds on a run-of-the-mill desktop PC. The paper presents the methodology, quantifies the computational time requirements and accuracy of both the g-function and the resulting designs.

1. INTRODUCTION

A common method for design of ground heat exchangers used with ground-source heat pump systems is based on simulations of the ground heat exchanger at different candidate depths. The simulations require anticipated ground heat extraction and rejection loads, ground thermal properties, details about the borehole heat exchanger design (e.g. borehole diameter, pipe sizes, flow rates, grout thermal properties), configuration (e.g. number of boreholes and horizontal positions) and finally depth of the boreholes. The commonly used approach (Spitler 2000, OSU 2016, BLOCON 2017) is to adjust the depth to give the smallest depth for which the user-specified maximum and minimum heat pump entering fluid temperatures will be exceeded.

Keeping in mind that determining the required depth for a single configuration may require approximately 10 iterations, and often multiple configurations must be evaluated during the design process, the simulations must be fast, on the order of a few seconds or less. The only practical method for performing these simulations with adequate speed involves the use of thermal response functions known as g-functions, originally developed by Prof. Johan Claesson and his graduate students. (Claesson and Eskilson 1985, 1988, Eskilson and Claesson 1988, Hellström 1991) Eskilson (1986) developed a computer code that can calculate g-functions. Libraries developed with this code are used by GLHEPRO and EED. The code is not publicly available. More recently, Cimmino (Cimmino 2018a, b, 2019a, b) developed an open-source tool, pygfunction, for computing g-functions. Cook and Spitler (2021) found that memory requirements of pygfunction could become excessive when g-functions were calculated for more than a few hundred boreholes. This led them to develop a C++ implementation (cpgfunction) with significant restructuring that allowed the memory to be reduced by approximately a factor of 8, while maintaining similar speeds to pygfunction.

Fast methods for calculating g-functions are of interest for design of ground heat exchangers, particularly for configurations with irregularly placed boreholes. These configurations are not found in libraries of g-functions. As shown by Spitler et al. (2020) irregular configurations that wrap around buildings instead of being confined to a standard (library) rectangular configuration may save significant drilling costs. An example in the paper, for a cooling-dominated office

building in Atlanta, saved over 40% in required drilling.

Speedy g-function calculation is needed for two aspects of the ground heat exchanger design: rapid selection of a configuration and sizing (determining the required depth) of a selected configuration. Automated selection of irregular configurations has not been possible in commercially available design tools but Cook (2021) reports on a range of configuration selection algorithms that make use of fast g-function calculations.

Late in 2021, Prieto and Cimmino (2021) published the equivalent borehole method (EBM) using a hierarchical agglomerative clustering method. Prieto and Cimmino's work is aimed at the same goal as this paper although the approach is very different. In limited testing, our method is faster than the EBM, up to about 300 boreholes, and the EBM is faster above 300 boreholes.

2. METHODOLOGY

The methodology employed here uses what is sometimes called the stacked finite line source (SFLS) method. Each borehole is discretized into multiple segments. The method is aimed at computing g-functions for specific borehole depths. For any configuration, g-functions are computed for a range of depths, and then interpolation is used to find the g-function for a specific depth. As about 10 iterations are typically needed to determine the required depth, interpolation gives a significant speed increase compared to calculating g-functions for every depth guess used in an iteration. Cook (2021) evaluates different interpolation procedures and shows that the error can be reduced to below 1% with the use of at least 5 g-functions. Cook investigated different interpolation procedures and determined that a quadratic spline interpolation between g-functions gave the best accuracy.

The following sections describe the important aspects of the methodology in this paper.

2.1 Discretization

The method described in this paper makes use of three non-uniform segments per borehole. Until recently, pygfunction only supported dividing each borehole into a set of uniform-length finite line sources. In this paper, boreholes are divided into three segments, as shown in Figure 1. There is a center segment and two end segments of equal length. Thus, for a given depth of borehole, the discretization can be defined by one parameter, the end segment length (ESL).

2.2 Pre-tabulated FLS integral

Because sets of g-functions for different depths are calculated for use in an interpolation procedure, it is possible to pre-define the depths (referred to in this paper as "height") for which g-functions are calculated. The selected g-function heights are 24m, 48m, 96m, 192m, and 384m. The corresponding borehole radii are .075m, .075m, .075m, .08m, and .0875m. The burial depth currently used is 2m. Using pre-defined heights allows pre-calculation of the segment-to-segment response factors. A modified version of pygfunction (the version available at the time could not make use of non-uniform segments) is used to calculate segment-to-segment responses between each pair of segments in a system consisting of only two boreholes. These calculations are run for a variety of horizontal distances between the two boreholes, and all possible combinations of pairs based on vertical location of the segment. The resulting segment-to-segment response factors are stored in nine tables (which are stored to file). Each table has the associated response factors between a pair of segments in the system; an example is the response between the bottom segment on the top segment. Each row in the table contains the distance between the two boreholes for a particular response as well as the associated responses. The columns contain the responses for differing non-dimensional time values. The responses of each segment on the segments in its borehole are stored under a borehole distance of zero. Each set of tables is limited by the heights, depths, and radii for which the table entries were calculated.

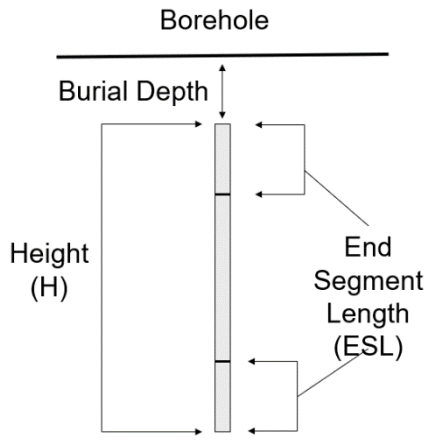

Figure 1: Borehole Discretization.

2.3 Boundary condition enforcement

To calculate g-functions for a specific field, the first step is calculating the distance between each pair of boreholes. From there, a segment-to-segment response matrix is built from the appropriate set of tables and the matrix of borehole distances. This is done by iterating through each borehole and interpolating the segment-to-segment response at each time interval based on the corresponding distance between the current borehole and each other borehole (with the segments response to itself also being read).

Next, the calculation sets up systems of equations for each time interval utilizing the matrix of segment-to-segment responses. Together, these are used along with the uniform borehole wall temperature boundary condition create the three complete systems of equations. The first holds the uniform borehole wall temperature condition (all boreholes must have the same wall temperature). The second corresponds to the heat extraction of the whole field being constant.

Lastly, the third system relates the segment responses to the individual rises in temperature for each segment. Cimmino and Bernier (2014) developed these equations which were implemented in pygfunction. The relevant information for the g-function calculation is the non-dimensional temperature rise for one segment (which is the same for every segment). The non-dimensional temperature rise for each time segment is returned as the g-function. The accuracy of this estimation is highly dependent on the selected ESL. The optimal ESL is dependent on several factors, so an in-depth investigation is necessary to get good approximations.

3. OPTIMAL ESL INVESTIGATION

In order to better understand the effect of ESL on the accuracy of the 3-segment approximation as well as variance in the optimal ESL for different fields and heights, a set of fields was generated. Specifically, fields ranging from a 50 to 1000 boreholes with varying shapes were generated. These fields were made using a "row-wise" bore field generation tool. This tool generates fields by using an outer polygon definition (representing a property boundary) and an inner polygon (representing a zone where no drilling is possible). The tool also takes an inter-row and intra-row spacing which it will use to place boreholes row by row (its namesake). The tool first determines how many rows in the y-direction will fit in a given property boundary with the given inter-row spacing. For each row, the tool starts with the specified intra-row spacing, but increases it, so that all space is utilized. Then, the tool iterates through each row. For each row, the tool determines if there is part of the row that is obscured by the interior polygon. Boreholes inside the no-drilling zone are removed. The no-drilling zone will divide some rows into "row segments". The spacing within each row segment is adjusted to place boreholes with a new, larger, uniform, intra-row spacing that makes full use of the available space.

Thousands of fields were generated by iterating through several types of internal and external polygons as well as sizes. Of these, 837 fields were selected to give a wide range of number of boreholes and field configurations. Four of these fields will be used as examples for presenting various results. These four cases are shown in Figures 2-5.

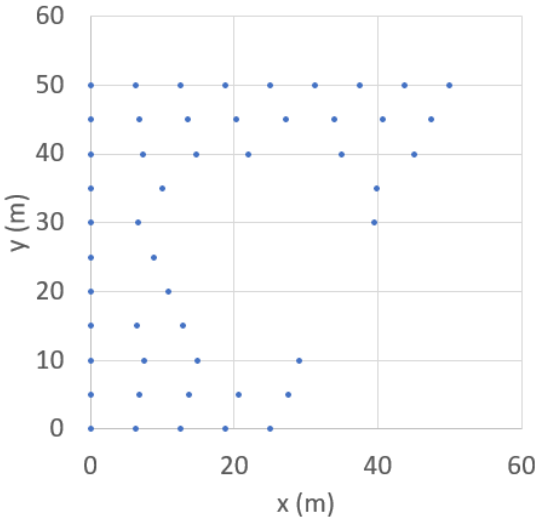

Figure 2: Example Case A, NBH = 50.

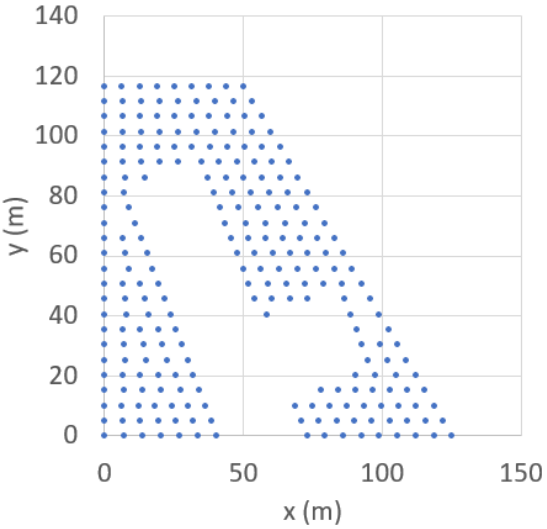

Figure 3: Example Case B, NBH = 245.

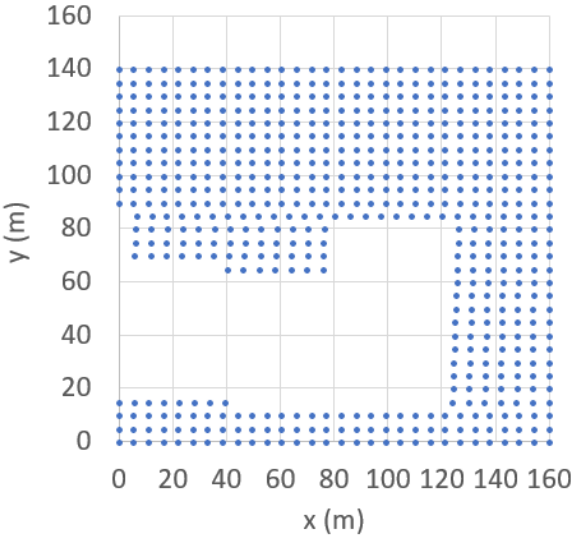

Figure 4: Example Case C, NBH = 600.

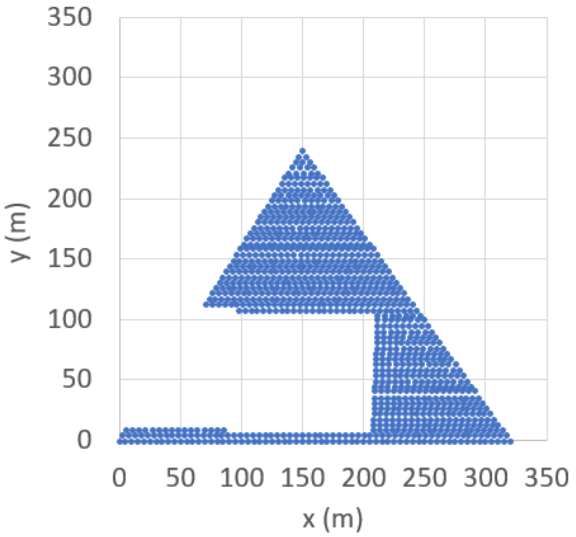

Figure 5: Example Case D, NBH = 997.

The performance of the g-function calculation method can be quantified with three important metrics: accuracy, memory usage, and calculation time. The timing and memory usage will be evaluated directly. However, the evaluation of accuracy will require more complex comparisons, as the final design requires interpolation between two g-functions.

The first comparison will demonstrate how ESL affects the accuracy of the approximation. The accuracy will be quantified using % RMSE when comparing the estimated g-functions (with a range of ESLs) with the results from cpgfunction. This will be done by using the accuracy results for the four example cases to discuss the general trends and reasoning for the recommended ESLs.

The second comparison, using the recommended ESL values, will look at a much larger set of configurations. This will be quantified by analyzing the % RMSE for five different heights (24m, 48m, 96m, 192m, and 384m) for all 837 different fields. This will give a sense of the overall g-function error.

The third comparison will demonstrate how error in the g-function propagates into error in the design. This will be characterized by visualizing the % difference in the design height of ground heat exchangers utilizing g-functions from cpgfunction and ones utilizing the 3-segment approximation. It should be noted that both methods utilize interpolation for the specific g-function calculation. The loadings are multiples of the loading of a typically office building in Atlanta. The design time utilized is 20 years. The ground heat transfer properties are set to values that would be typical for Atlanta. Three rounds of design comparisons were made. The first round focused on basing the loading to make each exchanger have a design height of approximately 100m. The second round similarly modified the loadings to create heat exchangers around 230m deep. The last round utilized a constant loading to create heat exchangers of widely varying height. Together, these three rounds of heat exchanger design comparisons demonstrate how the g-function error influences design error.

The fourth and last comparison investigates how the errors in g-functions are distributed. That is how the overall error (characterized as % RMSE) is typically manifested in the g-functions themselves. There are two ways that this is analyzed, both using the four example cases mentioned before. The first way visualizes the distribution by plotting the % error vs. non-dimensional time value for each of the example cases. The second method compares the % RMSE for each sample case with the % error at the largest non-dimensional time value calculated.

4. RESULTS

With the methodology behind the evaluation of the method discussed, the results from these comparisons will be reviewed. Cook and Spitler (2021) compared memory requirements for pygfunction and cpgfunction. Even with the 8-fold memory reduction in cpgfunction, a 1000 borehole field with 16 segments per borehole might still require 30GB of RAM, beyond the available RAM in many desktop computers. The 3-segment model reduces the RAM requirements so that g-functions may be computed for fields with a 1000 boreholes on a PC with 16GB RAM total. Therefore, no further investigation into memory usage was performed.

On average, the 3-segment model gives an improvement in timing by approximately one order of magnitude compared to cpgfunction. The timing results can be seen in Figure 6. These are calculated on Oklahoma State University's Pete Supercomputer Cluster. The nodes used had dual Intel "Skylake" 6130 CPUs as well as 96GB of RAM. Additionally, similar timing results were found (with the maximum calculation time for the 1000 NBH field being approximately 38s) utilizing a desktop pc with an i7-8700k CPU and 16GB of RAM. Something to note is that the calculation time for fields under an NBH of 400 took less than five seconds. This is notable as many designs utilize fields with less than this many boreholes. There are still major timing improvements for larger fields, but the calculation time can still be an obstacle to automated design that might involve evaluation of many configurations. Something else of note is the appearance of two bands in the timing data. This was caused by the fields being run on the supercomputing cluster at two separate times. There was a significant difference in the timing between the two (with the higher band being more consistent with the performance of the tested desktop pc). The exact cause behind the decreased performance is unknown but is likely related to the cluster rather than the algorithm.

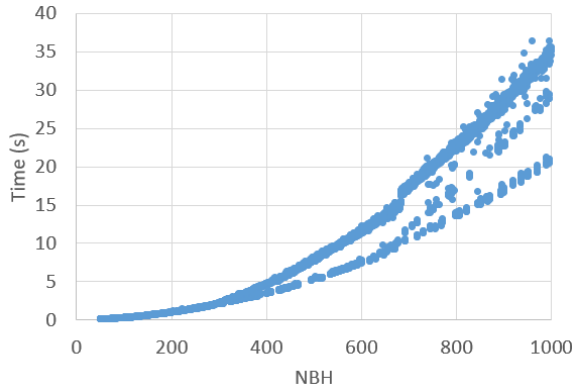

Figure 6: 3-Segment Model Timing Results

The sensitivity of the accuracy to the ESL was first investigated by plotting RMSE vs ESL, as shown in Figures 7-10. Each plot shows curves of RMSE vs. ESL for each computed depth. Each curve for a specific height and field shows an optimal (minimum RMSE) value, but there is not an optimal ESL for all scenarios. The optimal ESL value is dependent on the field shape, field spacing, borehole height, field NBH, and other factors. This means that recommended ESLs will still have some level of compromise (and better ESLs could be used for specific sets of fields). That said, there are some general trends that can be used to get ESLs that give pretty good results for a wide range of fields. One general trend is that the optimal ESL for a field (all heights) decreases with increasing NBH, but the rate of decrease is reduced with increasing NBH. This means that very small values of NBH will have optimal ESL values that are appreciably different from mid to large NBH fields. Fields with small numbers of boreholes tend to be more sensitive to the actual configuration, but the error due to deviating from the optimal ESL tends to be lower. (Compare RMSE in Figures 7 and 10.) This suggests that mid to large fields should be weighted over smaller fields when selecting ESL values to use for most cases. Another trend is in the overall shape of the %RMSE vs ESL curve. The curve has a sharper minimum with low heights, and a smoother curve with greater heights. Additionally, the absolute minimum RMSE moves slightly upward with greater depths.

With these trends taken into account, the recommended ESLs are as follows: 8m for a height of 24m, 12m for a height of 48m, 12m for a height of 96m, 11m for a height of 192m, and 11m for a height of 384m.

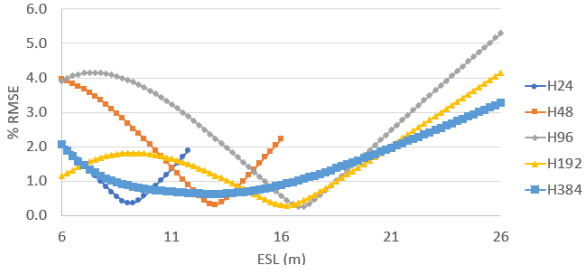

Figure 7: Case A, NBH 50, RMSE vs. ESL

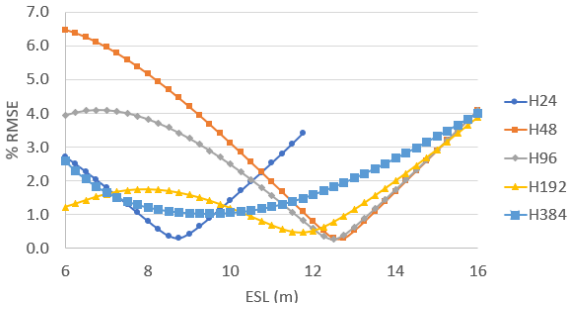

Figure 8: Case B, NBH 245, RMSE vs. ESL

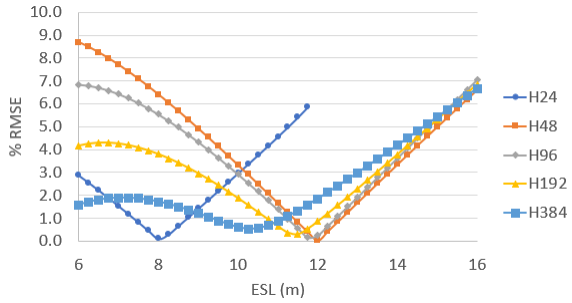

Figure 9: Case C, NBH 600, RMSE vs. ESL.

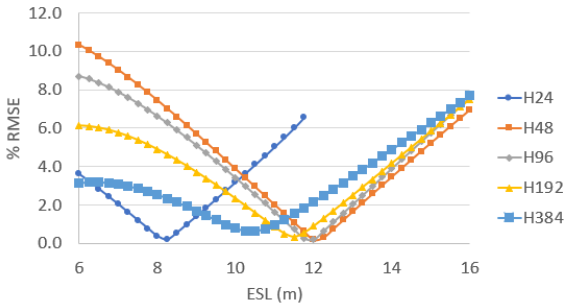

Figure 10: Case D, NBH 997, RMSE vs. ESL.

The second comparison serves to evaluate the validity of the recommended ESL values. Figure 11 illustrates %RMSE values for the 837 fields with all five heights selected. All configurations tested had an error less than 3.5% RMSE. For many of the configurations with heights less than 384m, the RMSE was less than 1%. Most of those fields with RMSEs larger than 1% are for NBH values less than 100. This is to be expected since fields with small NBH values have significantly different optimal ESLs.

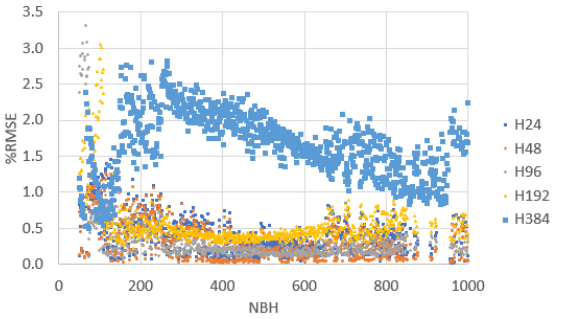

Figure 11: g-function RMSE vs. NBH for Five Selected Heights.

The third comparison, between design lengths, gives extremely good results. Figures 12-14 show the results

for the three rounds of design comparisons. For all cases tested, the percent difference in borehole height using 3-segment calculated g-functions vs. using cpgfunction was less than 1%. This difference can be positive or negative. Ideally, a simplified method like the 3-segment model would only have positive error leading to slightly conservative designs. However, the magnitude of the errors is quite small and the errors are smaller than many of the other uncertainties in the design process, so this approach should be acceptable.

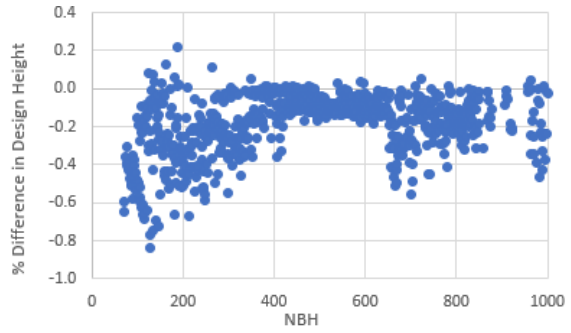

Figure 12: % Design Difference vs. NBH, 100m Target Depth.

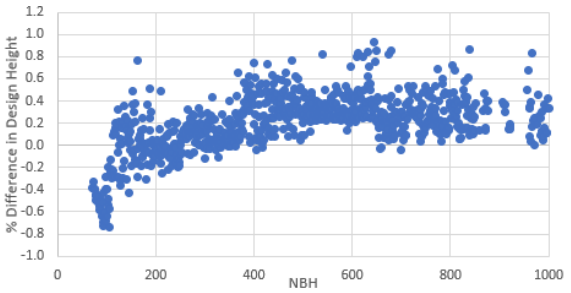

Figure 13: Design Difference vs. NBH, ≈230m Target Depth.

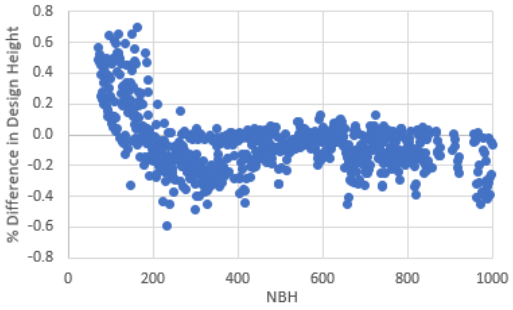

Figure 14: % Design Difference vs. NBH, Constant Loading.

The third round of comparisons, shown in Figure 14, where the design loads were a constant multiple of the Atlanta office building results in widely varying design depths. As illustrated in Figure 15, using this design loading with configurations between 50 and 1000 boreholes results in borehole depths between 40m and 384m. As also observed in the figure, the error in design height increases with the design height, but this is coincident with a decrease in the number of boreholes.

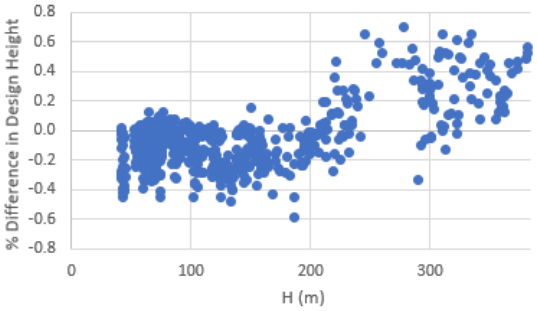

Figure 15: Design Difference vs. Design Height, Constant Loading.

Lastly, the relationship between the g-function RMSE and design difference is illustrated by Figure 16. The orange line represents the % design difference being equal to the % RMSE. The figure demonstrates that in most cases tested, the error in the design difference is lower than the g-function RMSE.

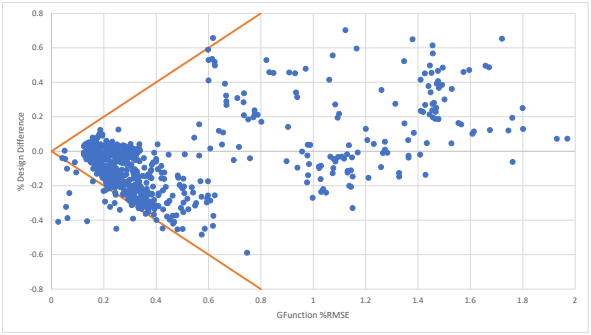

Figure 16: Design Difference vs. G-function RMSE, Constant Loading.

The final accuracy characterization gives some level of insight into how error is distributed throughout g-functions. Figures 17 and 18 shows the % error at each $\ln(t/t_s)$ value for the four example cases, at heights of 24m and 384m, respectively. The 3-segment estimate tends to overestimate the g-function at higher depths and tends to underestimate it at lower depths. The effects of borehole configuration, number of boreholes, and depth This trend becomes more complicated since the field also has a large effect on how close the g-function is. The most important takeaway is that the largest % error is still less than 5%.

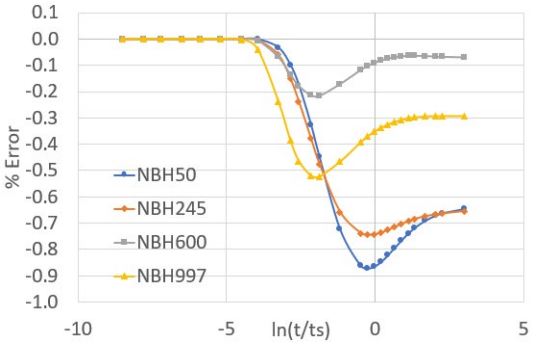

Figure 17: % Error vs $\ln(t/t_s)$, 24m Height.

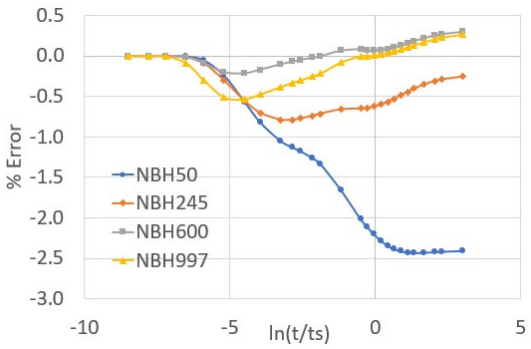

Figure 18: % Error vs ln(t/t_s), 96m Height

To give this error some additional context, Figures 19 and 20 compare the g-functions with the largest error from Figures 17 and 18 respectively. The figures demonstrate that even the maximum errors result in very small differences between the two g-functions.

Table 1 summarizes the RMSE errors for the g-functions, and the differences in design depths, comparing cpgfunction and the 3-segment method used here. In all cases, the difference in design height is less than 1%, compared to cpgfunction. Given the uncertainties in other aspects of the design – e.g. thermal conductivity of the ground is seldom known more accurately than ±10%, a 1% error in the design length should be acceptable for optimization of borefield configuration.

Based on these results, the 3-segment method is applicable to fields of varying regularity and NBH. For small fields, with, say, less than 50 boreholes, it may be preferable to calculate the g-functions with another method, since the optimal ESL is more sensitive to the configuration at low NBH values. Also, calculation times for small fields are comparatively short with conventional methods.

The 3-segment method relies on tuned values of the ESL, which depend on depth. It should also be possible to further increase the accuracy and range of the method by increasing the sophistication of the tuning method.

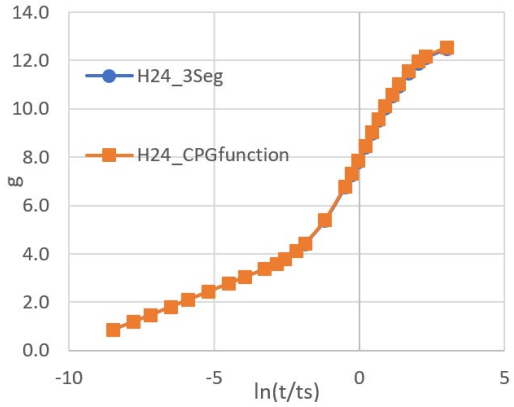

Figure 19: g-function Comparison, 24m Height, Case A.

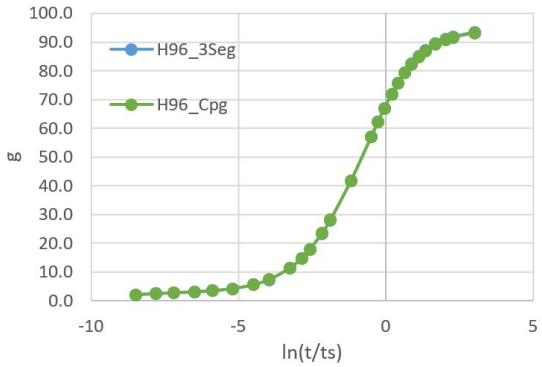

Figure 20: G-function Comparison, 384m Height, Case A.

Table 1: Example Case Error Summary

	24m Height		48m Height		96m Height		192m Height		384m Height		Design Comparisons			
NBH	RMSE (%)	ETE (%)	RMSE (%)	ETE (%)	RMSE (%)	ETE (%)	RMSE (%)	ETE (%)	RMSE (%)	ETE (%)	Design 1 Height (m)	Design 1 Difference (%)	Design 2 Height (m)	Design 2 Difference (%)
50	0.84	0.65	0.73	0.54	2.76	2.40	1.27	1.41	1.06	1.37	83.7	-0.75	168.7	-0.42
245	0.82	0.65	0.82	0.61	0.60	0.60	0.49	0.72	2.02	2.34	99.4	-0.43	203.3	-0.13
600	0.10	0.07	0.03	0.20	0.24	0.30	0.36	0.52	1.63	1.87	118.3	-0.02	248.9	0.40
997	0.40	0.29	0.24	0.20	0.20	0.26	0.54	0.69	1.70	2.00	132.8	-0.24	286.0	0.34

5. CONCLUSIONS

The 3-segment approach for calculating g-functions provides excellent accuracy at speeds that are much faster than any method previously available, at least before Prieto and Cimmino (2021) published the equivalent borehole model. The speed is fast enough that it should be suitable for automated design of borehole fields with hundreds of boreholes – covering almost all but the largest systems currently being installed. Except possibly for borehole fields with less than 50 boreholes, the errors in final design should be less than 1% in length. Nevertheless, this is within the uncertainty due to ground thermal properties, which is

on the order of ±5% for a ±10% uncertainty in ground thermal conductivity. It should be acceptable for automated design. It's likely that further tuning of the model, say, to have different ESL recommendations based on the number of boreholes would further improve the accuracy.

REFERENCES

BLOCON. 2017. "Earth Energy Designer (EED) Version 4 Update Manual." Retrieved February 13, 2019, from https://buildingphysics.com/eed-2/.

Cimmino, M. and Bernier, M. 2014. A semi-analytical method to generate g-functions for geothermal bore fields. *International Journal of Heat and Mass Transfer* 70: 641-650

Cimmino, M. 2018a. Fast calculation of the g-functions of geothermal borehole fields using similarities in the evaluation of the finite line source solution. *Journal of Building Performance Simulation* 11(6): 655-668.

Cimmino, M. 2018b. pygfunction: an open-source toolbox for the evaluation of thermal. *eSim 2018*, Montreál, IBPSA Canada. 492-501.

Cimmino, M. 2019a. "pygfunction GitHub Page." Retrieved October 24, 2019, from https://github.com/MassimoCimmino/pygfunction .

Cimmino, M. 2019b. Semi-Analytical Method for g-Function Calculation of bore fields with series- and parallel-connected boreholes. *Science and Technology for the Built Environment* 25(8): 1007-1022.

Claesson, J. and P. Eskilson. 1985. Thermal analysis of heat extraction boreholes. *Proceedings of 3rd International Conference on Energy Storage for Building Heating and Cooling ENERSTOCK 85*, Toronto (Canada), Public Works Canada. 222–227.

Claesson, J. and P. Eskilson. 1988. Conductive Heat Extraction To A Deep Borehole: Thermal Analysis and Dimensioning Rules. *Energy* 13(6): 509-527.

Cook, J. C. 2021. Development of Computer Programs for Fast Computation of G-functions and Automated Ground Heat Exchanger Design. M.S. Thesis, Oklahoma State University.

Cook, J. C. and J. D. Spitler 2021. Faster computation of g-functions used for modeling of ground heat exchangers with reduced memory consumption. *Building Simulation 2021*. Bruges, Belgium, IBPSA.

Eskilson, P. 1986. Superposition Borehole Model - Manual for Computer Code. *University of Lund*.

Eskilson, P. and J. Claesson. 1988. Simulation Model For Thermally Interacting Heat Extraction Boreholes. *Numerical Heat Transfer* 13(2): 149-165.

Hellström, G. 1991. Ground Heat Storage – Thermal Analyses of Duct Storage Systems - Theory PhD Doctoral Thesis, University of Lund.

OSU 2016. GLHEPro 5.0 for Windows - Users' Guide. *Oklahoma State University*, Stillwater.

Prieto, C. and M. Cimmino. 2021. Thermal interactions in large irregular fields of geothermal boreholes: the method of equivalent boreholes. *Journal of Building Performance Simulation* 14(4): 446-460.

Spitler, J. D. 2000. GLHEPRO -- A Design Tool For Commercial Building Ground Loop Heat Exchangers. *Fourth International Heat Pumps in Cold Climates Conference*, Aylmer, Québec.

Spitler, J. D., J. C. Cook and X. Liu 2020. A Preliminary Investigation on the Cost Reduction Potential of Optimizing Bore Fields for Commercial Ground Source Heat Pump Systems. *Proceedings, 45th Workshop on Geothermal Reservoir Engineering*. Stanford, California, Stanford University.

Acknowledgements

The research described in this paper was funded by the Center for Integrated Building Systems at Oklahoma State University.